Noise Figure of Watt-Class Ultralow-Confinement Semiconductor Optical Amplifiers

William Loh, *Student Member, IEEE*, Jason J. Plant, Jonathan Klamkin, *Member, IEEE*, Joseph P. Donnelly, *Life Fellow, IEEE*, Frederick J. O'Donnell, Rajeev J. Ram, *Senior Member, IEEE*, and Paul W. Juodawlkis, *Senior Member, IEEE*

***Abstract*— We investigate the noise figure (NF) of high-power semiconductor InGaAsP optical amplifiers (SOAs) based on the slab-coupled optical waveguide (SCOW) concept having both ultralow optical confinement ($\Gamma \sim 0.5\%$) and low optical loss ($\alpha_i \sim 0.5$ cm^{-1}). At 1550 nm and 5-A current bias, the NF of SCOW amplifier (SCOWA) is 5.5 dB, and the small-signal gain and saturation output power are 13 dB and 0.8 W, respectively. A minimum NF of 4.5 dB is achieved at 2-A bias. These NF results represent the lowest reported for a packaged SOA. Using the measured NF, the population inversion factor (n_{sp}) of the SCOWA was also estimated. The derived n_{sp} values indicate that intervalence band absorption loss, carrier heating, and quasi-bound higher order modes may ultimately limit the noise performance of InGaAsP SOAs.**

***Index Terms*— Noise, noise measurement, power amplifiers, quantum-well devices, semiconductor optical amplifiers.**

I. Introduction

THE noise figure (NF) of an optical amplifier is an important figure of merit used to characterize the amplifier's potential for low-noise performance. Typically, low NF is needed for preamplifier and inline amplifier applications, which generally require the amplifier to be polarization insensitive. Low NF is also important for the realization of low-noise lasers because a laser's relative intensity noise (RIN) and linewidth are both intrinsically related to the NF of the laser's optical gain medium. For integrated master oscillator power amplifier systems, low noise, high power, and narrow-linewidth coherent sources can be realized.

Considerable research has been performed on semiconductor optical amplifiers (SOAs) due to their small size, low weight, high power efficiency, and their potential for photonic integration [1]–[3]. A new class of SOAs, referred to as slab-coupled optical waveguide amplifiers (SCOWAs), show much promise as they exhibit high saturation power, reasonable gain, and low NF with both low coupling loss and low internal loss. These unique properties are achieved using a low optical confinement design ($\Gamma \sim 0.5\%$) that allows for mode sizes of 5×7 μm^2, internal losses $\alpha \sim 0.5$ cm^{-1}, and fiber-coupling efficiencies $\eta_c > 90\%$ [4].

Previously, we reported on the characteristics of a packaged SCOWA operated at 1.54 μm wavelength and 5 A bias, demonstrating 13 dB gain, >100 nm gain bandwidth, 0.8 W saturation output power, and 5.5 dB NF [5]. The purpose of this paper is to extend our measurements and to analyze the specific mechanisms that lead to NF degradation in SCOWAs specifically and SOAs in general. To our knowledge, the work presented in this paper provides the first thorough analysis of the limitations to SOA noise performance. We first verify the accuracy of our previous optical-domain NF measurements by using an independent electrical-domain technique. We then use the NF measurements to derive the population inversion factor (n_{sp}) under various operating conditions of current and wavelength. Comparisons between n_{sp} determined from the SCOWAs NF and n_{sp} found from the SCOWAs measured *I–V* characteristic reveal that effects of intervalence band absorption (IVBA) losses and carrier heating may ultimately limit the noise performance of SOAs at 1.55 μm. In addition, we also observe the presence of quasi-bound higher order transverse modes at shorter wavelengths. We believe that these higher order modes reduce the coupling efficiency, thereby causing the SCOWA NF to increase. This multimode NF degradation may affect any waveguide SOA that operates across a wide spectral bandwidth.

II. Packaged SCOWA Description

The structure of the fiber-pigtailed SCOWA studied in this paper (Fig. 1) consists of an n-InP buffer layer (0.2 μm, 10^{18} cm^{-3} S), an n-InP cladding layer with a graded doping profile (1 μm, 1.0–0.2 $\times$ 10^{18} cm^{-3} S), a thick lightly n-doped InGaAsP waveguide ($h = 4.9$ μm, 5×10^{16} cm^{-3} S, $\lambda_G = 1.03$ μm), a nominally undoped multiple-quantum-well (MQW) active region, a p-AlInAs electron blocking layer (0.025 μm, 5×10^{17} cm^{-3} Zn), a p-InP cladding layer with a graded doping profile (1 μm, 2–8 $\times$ 10^{17} cm^{-3} Zn), a p-InP cap layer (0.6 μm, 10^{18} cm^{-3} Zn), and a p+ InGaAs contact layer (0.2 μm, 10^{19} cm^{-3} Zn). The device structure was grown on an n-type (100) InP substrate using organometallic

Manuscript received June 22, 2010; revised August 19, 2010; accepted September 30, 2010. Date of current version December 10, 2010.

W. Loh is with the Electroopical Materials and Devices Group, MIT Lincoln Laboratory, Lexington, MA 02421 USA, and also with MIT Department of Electrical Engineering and Computer Science, Massachusetts Institute of Technology, Cambridge, MA 02139 USA (e-mail: william.loh@ll.mit.edu).

J. J. Plant, J. Klamkin, J. P. Donnelly, F. J. O'Donnell, and P. W. Juodawlkis are with the Electroopical Materials and Devices Group, MIT Lincoln Laboratory, Lexington, MA 02421 USA (e-mail: plant@ll.mit.edu; klamkin@ll.mit.edu; donnelly@ll.mit.edu; odonnell@ll.mit.edu; juodawlkis@ll.mit.edu).

R. J. Ram is with the Department of Electrical Engineering and Computer Science, Massachusetts Institute of Technology, Cambridge, MA 02139 USA (e-mail: rajeev@mit.edu).

Digital Object Identifier 10.1109/JQE.2010.2085422

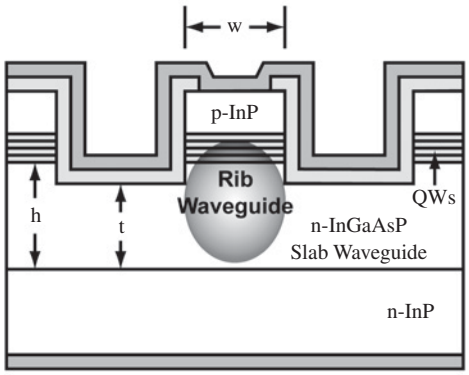

Fig. 1. Diagram of SCOWA cross section.

vapor-phase epitaxy. The active region contains five 8-nm-thick compressively strained (1%) InGaAsP QWs with peak photoluminescence wavelength at 1.53 μm. The InGaAsP barrier and bounding layers ($\lambda_g = 1.21$ μm, tensile strained (-0.3%), and 8 and 12 nm thick, respectively [5], [6].

Ridges of $w = 5.8$ μm width were formed by etching 0.9 μm into the InGaAsP slab ($t = 4.0$ μm). The reflectivity of the SCOWA facets was minimized by a combination of 5°-oriented (110) angle cleaving followed by antireflection coating. The total device length was 1 cm. Careful selection of the refractive index of the waveguide along with proper design of thickness and width allowed us to achieve a large optical mode having low overlap with both the active region (low Γ) and p-InP layers (low α) (see Fig. 1). Single-mode operation in the SCOWA is obtained by virtue of the fact that only the fundamental mode experiences significant overlap with the MQWs with the higher order modes suffering a net loss [7].

III. NF Analysis and Results

The NF expresses the signal-to-noise ratio (SNR) degradation from input to output upon propagation through an amplifier [8]

$$NF = \frac{SNR_{in}}{SNR_{out}}. \tag{1}$$

Noise in optical amplifiers results from the mixing of incoherent spontaneously emitted photons with signal photons. The travelling-wave equation describing this process is given by

$$\frac{dN_p}{dz} = (\Gamma g - \alpha) N_p + \Gamma g \frac{n_{sp}}{V_{ph}}. \tag{2}$$

The solution of (2) is

$$N_p(L) = N_{p,in} G_{amp} + \frac{\Gamma g}{\Gamma g - \alpha} \frac{n_{sp}}{V_{ph}} \left(G_{amp} - 1\right) \tag{3}$$

where the signal and noise photons are represented by the first and second term on the right-hand side respectively, and N_p is the total photon density, Γ is the optical confinement factor, g is the material gain coefficient, α is the absorption coefficient, and V_{ph} is the photon volume. G_{amp} is the small-signal chip gain given by

$$G_{amp} = e^{(\Gamma g - \alpha)L}. \tag{4}$$

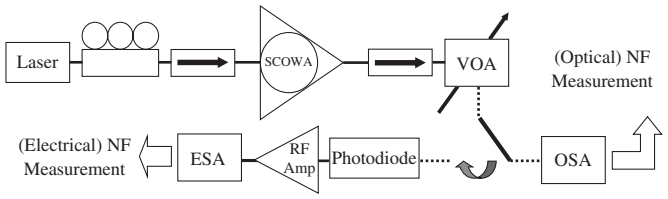

Fig. 2. Optical and electrical NF measurement system.

In (3), n_{sp} is the population inversion factor and is related to the electron (f_c) and hole (f_v) Fermi occupancy factors by

$$n_{sp} = \frac{f_c (1 - f_v)}{f_c - f_v}. \tag{5}$$

In an ideal amplifier, $n_{sp} \sim 1$, which can be achieved at a given photon energy if all the conduction band states are filled ($f_c \sim 1$) or all the valence band states are empty ($f_v \sim 0$). Equation (5) can be reformulated in terms of the quasi-Fermi level separation energy (ΔE_F) as [9]

$$n_{sp} = \frac{1}{1 - e^{\left(\frac{E_{ph} - \Delta E_F}{kT_c}\right)}} \tag{6}$$

where E_{ph} is the photon energy, k is the Boltzmann constant, and T_c is the carrier temperature. This equation assumes a thermal distribution of carriers within the SOA and is expected to be valid for the continuous-wave steady-state operating conditions used in our experiments.

The NF of an optical amplifier is a measure of the amplified spontaneous emission (ASE) noise relative to the signal generated by the amplifier. The ASE can be found by formulating the second term of (3) in terms of optical power units through

$$P_{ASE} = \frac{\Gamma g}{\Gamma g - \alpha} n_{sp} h\nu (G_{amp} - 1) B_o \tag{7}$$

where B_o is the optical bandwidth, h is the Planck constant, and ν is the optical frequency. The NF of the SCOWA was measured independently using both optical and electrical domain techniques. The system setup used to perform both measurements is illustrated in Fig. 2. In both configurations, the optical output of a tunable laser source is sent through a fiber-based polarization controller and an optical isolator before being amplified by the SCOWA. The amplified output passes through an optical isolator and a variable optical attenuator (VOA). In the optical measurement, an optical spectrum analyzer (OSA) is used to detect and process the amplified signal. Alternatively, in the electrical measurement, a photodiode converts the signal into an electrical signal that is amplified by an radio frequency (RF) amplifier. The spectrum of the amplified electrical signal is observed with an electrical spectrum analyzer (ESA).

The optical technique is performed by measuring the gain and ASE properties of the amplifier. The gain is found by taking the ratio of the signal with the amplifier inserted and removed from the system. The ASE is determined from the subtraction of the interpolated noise floor with amplifier inserted and removed. With these two measurements, NF is given by [8]

$$NF = \chi \left(\frac{K \gamma P_{ASE,measured}}{G h \nu B_o} + \frac{1}{G} \right) \tag{8}$$

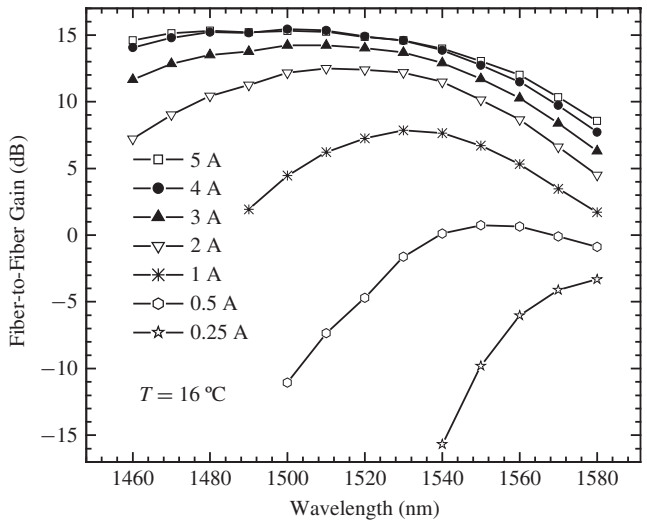

Fig. 3. Packaged SCOWA gain spectra for 0.25–5 A bias under small-signal input conditions. The temperature was maintained at $T = 16$ ºC.

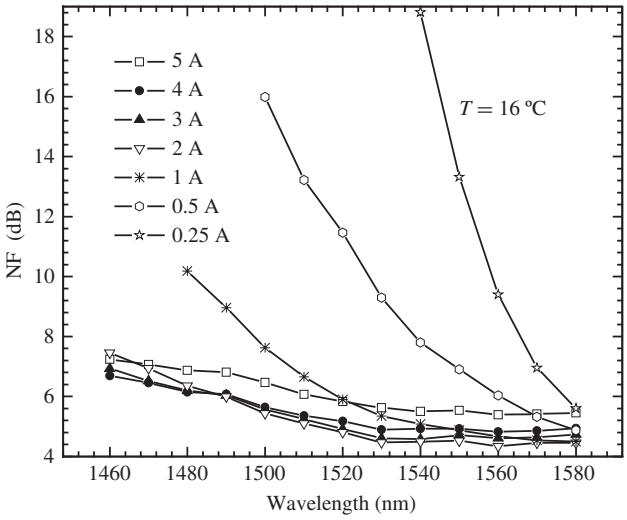

Fig. 4. Packaged SCOWA NF spectra measured using optical techniques for 0.25–5 A bias under small-signal input conditions. The temperature was maintained at $T = 16$ ºC.

where $P_{ASE,measured}$ is the measured ASE noise power, and G is the SOA gain including the input and output coupling losses. K is a factor correcting for the polarization dependence of the amplifier. For SOAs emitting primarily in the transverse electric (TE) polarization, K is given by

$$K = \frac{2}{1 + P_{ASE,TM}/P_{ASE,TE}}. \tag{9}$$

Here $P_{ASE,TM}$ and $P_{ASE,TE}$ represent the ASE in the transverse magnetic (TM) and TE polarizations, respectively [10]. The TM and TE ASE in (9) should be interchanged for SOAs emitting primarily in the TM polarization. Amplifiers that are strongly polarization sensitive have $K \sim 2$, whereas amplifiers that are insensitive to polarization have $K \sim 1$. The parameter γ in (8) can be represented as

$$\gamma = \frac{P_{sig\_out}}{P_{sig\_measured}} \tag{10}$$

and accounts for the total optical loss in the output path from the amplifier output up to and including the OSA. P_{sig_out} is the signal at the output of the amplifier, and $P_{sig\_measured}$ is the signal measured at the OSA. Finally, χ in (8) corrects for the polarization rotation of the optical signal before coupling to the SOA and is given by (see Appendix)

$$\chi = \frac{G_{detuned}}{G_{aligned}}. \tag{11}$$

Here, $G_{aligned}$ and $G_{detuned}$ represents the gain measured when the signal polarization is aligned and detuned, respectively, relative to the amplifier. Significant polarization detuning can occur when a fixed input signal is used to probe the gain over a large wavelength range. For polarization-sensitive SOAs, rotation of the signal due to dispersion causes NF to appear higher. The gain and NF spectra of the packaged SCOWA measured using the optical technique were previously reported in [5]. In Figs. 3 and 4 we show again these results, which will be used in later sections to determine n_{sp} of the amplifier. The NF of the SCOWA is 5.5 dB operated at 5 A bias and $\lambda = 1550$ nm. The NF decreases to a minimum of 4.5 dB when the current is reduced to 2 A but increases again for even lower biases. Over the entire wavelength range tested, the NF of the SCOWA was <7.5 dB when operated at 5 A. The increase in NF with bias is commonly observed in SOAs reported in the literature [11], [12] but is usually attributed to "thermal effects." In this paper, we identify and quantify the different mechanisms that lead to NF degradation.

To confirm the results of our optical measurements, we performed independent electrical NF measurements on the packaged SCOWA. The electrical measurements directly determine the total noise within the detected signal, which can be used to assess the NF of the amplifier. The electrical NF measurements were calibrated using the RIN transfer standard method [13], [14]. A comparison of results between NF measurements at 5 A performed using the optical and electrical domain techniques is shown in Fig. 5. The agreement is better than 0.1 dB over the tested wavelength range (1460–1580 nm) due to the precise calibration of both measurements. To our knowledge, the measured NFs of the SCOWA are the lowest demonstrated to date for a packaged SOA. Erbium-doped fiber amplifiers (EDFAs) can achieve an even lower NF, with some EDFAs reaching the ideal 3-dB limit. However, these low NFs can only be achieved in high-gain low-power configurations. High-power EDFAs typically exhibit NF $\sim$ 4–6.5 dB, which is comparable to that of an SCOWA [15].

Typical SOAs have NF between 7 and 11 dB [16]. The large NF of conventional SOAs is attributed to their low coupling efficiency, high internal loss, and large optical confinement. The effects of low coupling efficiency and high optical loss result in NF degradation through signal attenuation. High optical confinement can lead to lower population inversion resulting from saturation of the front end of the amplifier [17]. The SCOWAs novel large optical mode structure effectively solves these problems, thus allowing low NF to be achieved. The advantages of the SCOWA structure in NF performance

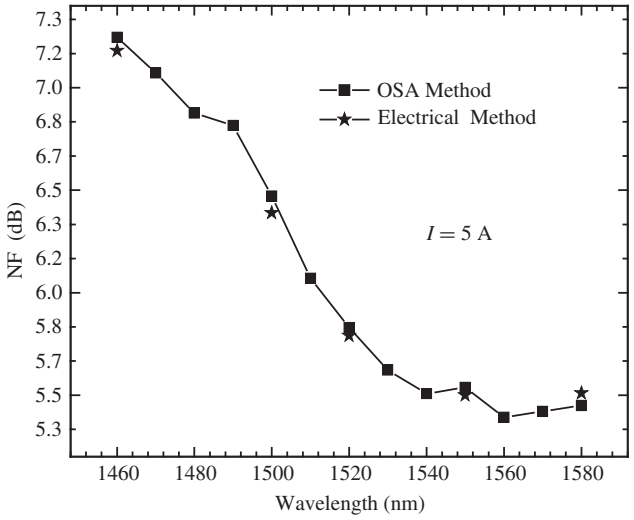

Fig. 5. Packaged SCOWA NF measured using optical (squares) and electrical (stars) techniques at 5 A bias under small-signal input conditions. The temperature was maintained at $T = 16$ ºC.

are clearly seen in (12)

$$NF = \frac{1}{\eta_{in}} \frac{2n_{sp}(G_{amp}-1)}{G_{amp}} \frac{\Gamma g}{\Gamma g - (\alpha_i + \alpha_{IVBA})} + \frac{1}{G_{amp}\eta_{in}\eta_{out}} \tag{12}$$

where η_{in} and η_{out} are the input and output coupling efficiencies, α_i is the carrier-independent internal absorption coefficient, and α_{IVBA} is the absorption coefficient resulting from IVBA. Equation (12) shows that NF is minimized by the combination of high input coupling efficiency (η_{in}), low saturation (i.e., low n_{sp}), and low optical loss ($\alpha_i + \alpha_{IVBA}$). Free carrier absorption losses are neglected since IVBA effects are dominant in InP. Equation (12) results from direct substitution of (7) into (8) after accounting for η_{in}, η_{out}, K, γ, and χ in P_{ASE}. Equations (7) and (12) are usually reported in the literature with $\Gamma g/(\Gamma g - (\alpha_i + \alpha_{IVBA}))$ excluded. This factor was first derived by Henry using the Green's function method [18]. Here, we have shown that this same factor can be found by solution of the SOA travelling-wave (2).

IV. Population Inversion Factor Analysis and Results

The population inversion factor (n_{sp}) describes the ratio of the spontaneous emission rate to the single-photon stimulated emission rate for an optical gain medium. We compute n_{sp} using two independent measurement techniques. We first extract n_{sp} from NF measurements since noise and spontaneous emission are inherently related through (12). We also determine n_{sp} using measured diode *I–V* characteristics by relating the junction voltage to the inversion of the amplifier. The values of n_{sp} found using both methods are compared for the purposes of understanding the increase in NF observed in Fig. 4 at higher current biases. With the NF method, we estimate n_{sp} using (12) and Figs. 3 and 4 assuming the following parameter values: $\eta_{in} = \eta_{out} = 90\%$, $\alpha_i = 0.5$ cm^{-1}, $\alpha_{IVBA} = 0$ cm^{-1}, and $\Gamma = 0.5\%$. We use (6) to estimate n_{sp} from *I–V* measurements of the amplifier diode. In this technique, the diode voltages are used to calculate n_{sp} from

$$\frac{\Delta E_F}{q} = V_{applied} - IR_{series} \tag{13}$$

with series resistance accounted for. In (13), q is the elementary charge, I is the supplied current, and $V_{applied}$ and R_{series} are the total applied voltage and series resistance between the power source terminals, respectively. Fig. 6 illustrates the estimated n_{sp} of the SCOWA found using both NF and *I–V* techniques as a function of wavelength for current biases of 0.5, 1, 3, and 5 A. The agreement is excellent between the two methods at 0.5 A bias, but becomes increasingly worse at higher current biases.

We use (12) to evaluate the cause of this difference in estimated n_{sp}. The value of G_{amp} was determined by accounting for the coupling loss in the measured values of fiber-to-fiber gain (G). Γg is calculated from G_{amp} using the measured internal loss values and a low-bias estimate of the IVBA loss ($\alpha_{IVBA} = 0$ cm^{-1}). The only parameters left that can contribute to the difference in estimated n_{sp} are then η_{in}, η_{out}, and α_{IVBA}. The carrier temperature (T_c) is used to compute n_{sp} in the *I–V* method and may also be a source of error. However, none of the individual parameters can account for the difference in n_{sp}. For example, on the long wavelength side of the n_{sp} spectra, a decrease in η_{in} and η_{out} from 90% to 66% would be required to match the n_{sp} measurements. This large decrease is not consistent with the expected coupling performance in SCOWA devices. In addition, since $T_c = 16$ °C was assumed in the n_{sp} calculations, the n_{sp} determined using *I–V* results may be inaccurate when the carrier temperature increases. However, carrier heating primarily impacts the inversion at shorter wavelengths, and unreasonable temperatures ($T_c > 850$ K) are needed to explain the large differences at longer wavelengths. Finally, an increase in the IVBA loss alone cannot account for the wavelength-dependent n_{sp} deviations seen in Fig. 6. This is true because IVBA losses decrease rather than increase at shorter wavelengths [19]. We will show that pump-current related degradation in α_{IVBA}, T_c, and coupling efficiency can all contribute to increased NF performance in 1.55-μm SOAs.

A. IVBA Loss

One of the causes of the difference in the estimated n_{sp} spectra shown in Fig. 6 is attributed to IVBA. It is well known that IVBA effects are greatly suppressed in compressively strained QW structures [20]–[22]. This suppression is due to the higher curvature of the heavy-hole (hh) band under compressive strain, which results in IVBA transitions between states having negligible hole concentration. However, under high bias conditions, the carrier concentration and temperature both increase, and significant concentrations of carriers occupy the 3-D barrier states. The IVBA losses of these barrier states are much larger than that of the strained wells. This effect has been use to explain the temperature dependence of InGaAsP QW lasers [23], [24].

TABLE I
CALCULATED SCOWA IVBA AND TEMPERATURE PARAMETERS

Current (A)	0.25	0.5	1	2	3	4	5
Carrier density (cm^{-3})	1.3×10^{18}	1.9×10^{18}	2.6×10^{18}	3.4×10^{18}	4.1×10^{18}	4.6×10^{18}	5.0×10^{18}
Total loss (cm^{-1})	0.50	0.50	0.50	0.58	0.78	0.98	1.40
IVBA loss (cm^{-1})	~ 0	~ 0	~ 0	0.08	0.28	0.48	0.9
IVBA cross section (cm^2)	–	–	–	4.7×10^{-18}	1.4×10^{-17}	2.1×10^{-17}	3.6×10^{-17}
Carrier temperature (K)	289	289	289	310	350	400	450

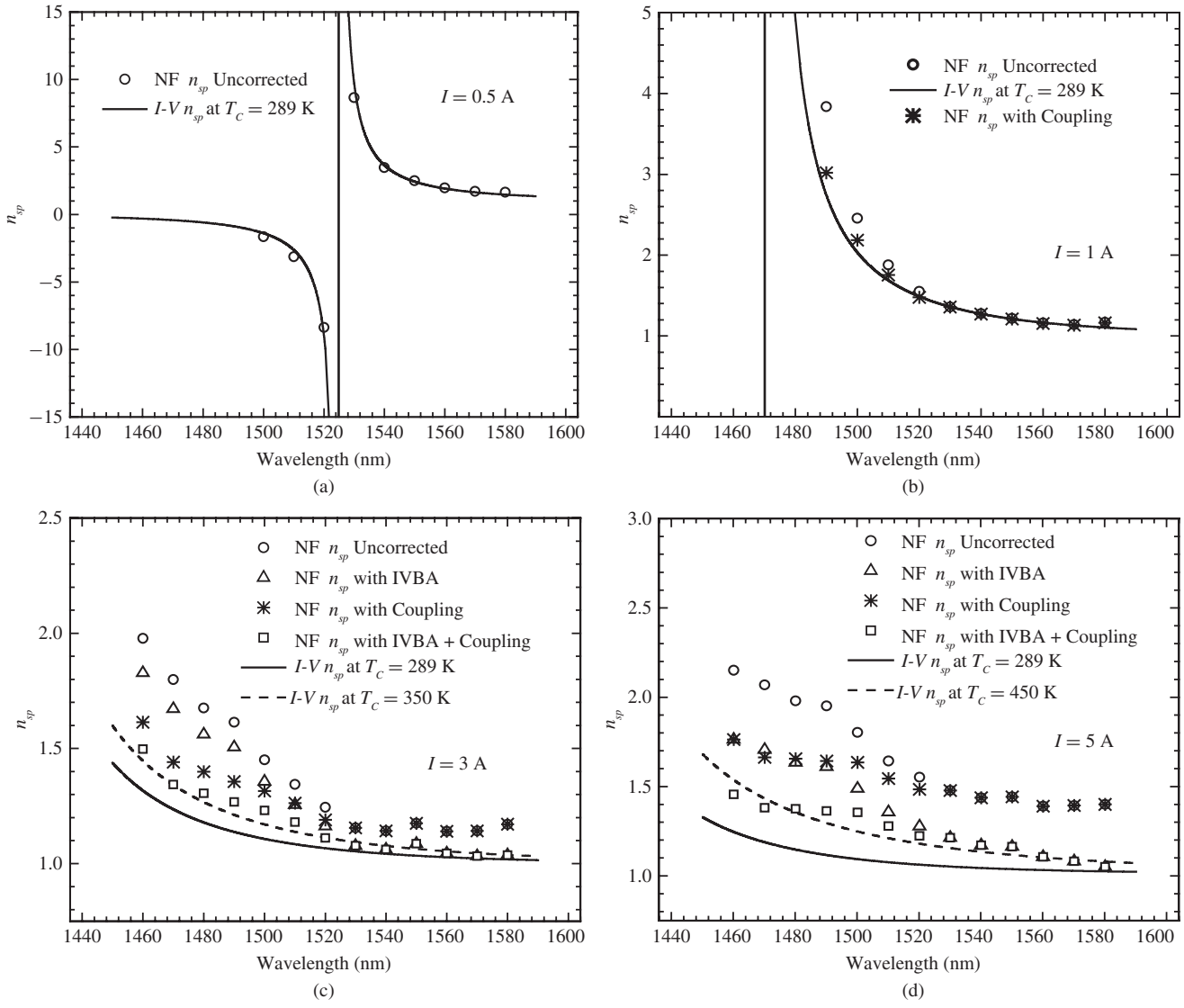

Fig. 6. SCOWA population inversion factor (n_{sp}) calculated using NF measurements (open circles) and *I–V* measurements (solid line) for (a) 0.5 A; (b) 1 A; (c) 3 A; and (d) 5 A bias. The n_{sp} calculated from NF measurements taking into account only IVBA effects (open triangles), only coupling loss effects (open stars), and both IVBA and coupling loss effects (open squares) is also shown. The dashed line indicates the n_{sp} calculated from *I–V* measurements and including carrier heating.

Table I shows the calculated SCOWA IVBA cross section (σ) as a function of bias. σ was derived using simulated carrier densities along with extracted values of α_{IVBA} from curve fitting. The carrier density was estimated by solution of the steady-state carrier rate equation, and the IVBA losses were determined by minimizing the difference between the *I–V* and NF n_{sp} values at the longer wavelengths with α_{IVBA} and T_c as independent parameters. For a given current bias, the IVBA loss was assumed to be approximately the same over all wavelengths in the range tested. This approximation greatly simplifies our analysis, and we calculate the resulting maximum error in α_{IVBA} to be $<10\%$. Coupling efficiency degradation was not included in the fitting since it is expected to be negligible at longer wavelengths as will be explained

later. The calculated σ increases from $\sim 4.7 \times 10^{-18}$ cm^2 to $\sim 3.6 \times 10^{-17}$ cm^2 as current increases to 5 A as seen in Table I. In these calculations, we assume Γ of the barriers to be approximately the same as Γ of the QWs since their total thicknesses are similar. The small σ values at low bias currents agree with findings in the literature [20]. Similarly, our calculated cross section for 5 A tends toward the bulk semiconductor values ($\sigma \sim 5 \times 10^{-17}$ cm^2) reported in the literature [23]. The open triangles in Fig. 6(c) and (d) shows the effect of IVBA on n_{sp} derived from NF measurements. The n_{sp} curves still disagree with the *I–V* measurements, especially at shorter wavelengths. We note that the current biases in Fig. 6(a) and (b) were too small to observe significant IVBA loss.

B. Carrier Heating

Carrier heating arises as a result of stimulated emission and Auger recombination processes [25], [26]. Each stimulated emission event removes an electron–hole pair having an energy difference less than the quasi-Fermi level separation, resulting in an increase in the effective carrier temperature. Similarly, each Auger recombination event removes a low-temperature electron–hole pair and increases the energy of a third carrier. The effect of carrier heating is increased by the presence of excited QW states since the population inversion will be even lower. Calculation of the energy levels for our material system yields one conduction-band state, four hh states, and one light-hole state. The transition wavelengths of the hh1 and hh2 states are 1576 and 1519 nm, respectively, and the other transitions are outside the measured wavelength range. The hh2 state should not contribute significantly to radiative transitions because of a small overlap of the envelope with the conduction-band state. As a result, the increased density of states from the hh2 state increases the carrier density required to achieve a specific gain. This increases the value of n_{sp}, particularly at shorter wavelengths.

The effects of carrier heating were evaluated using (6). It can be verified that the presence of excited states decreases ΔE_F, thereby increasing the temperature sensitivity of n_{sp}. As mentioned earlier, T_c was determined at each bias current in conjunction with α_{IVBA} by appropriate fits to the long wavelength n_{sp}. The values for T_c are provided in Table I and match well with T_c reported in the literature for 1.55-μm wavelength operation SOAs [25]. The effect of T_c on n_{sp} (dashed lines) is illustrated in Fig. 6(c) and (d). Carrier heating is seen to primarily increase n_{sp} at the shorter wavelengths. However, the combination of carrier heating and IVBA is not sufficient to account for all of the difference between the NF and *I–V* n_{sp} values. We note again that the current biases were too small to produce any observable carrier heating effects in Fig. 6(a) and (b).

C. Wavelength-Dependent Coupling

We attribute the remaining error between the values of n_{sp} determined using NF and *I–V* methods to be due to spectral variations in the coupling efficiency. We believe that this variation results from the presence of higher order transverse modes within the SCOWA waveguide. At shorter wavelengths, the higher order modes become quasi-bound modes that exhibit larger overlap with the gain. Coupling into these higher order modes increases as the modes become more bounded, resulting in a decrease in input coupling into the fundamental mode. To investigate this loss mechanism, we imaged the near-field output of an unpackaged benchtop SCOWA device that was seeded by a tunable laser source. The near-field images were captured at low biases (0.2 A) for wavelengths 1500–1525 nm where the intensities of the fundamental and higher order modes were nearly equal. The calculated coupling efficiencies between the near-field modes and a measured lensed-fiber mode are shown in Fig. 7 as a function of wavelength. The pictures taken of the near-field modes corresponding to wavelengths of 1519, 1521, 1523, and 1525 nm are also given in Fig. 7.

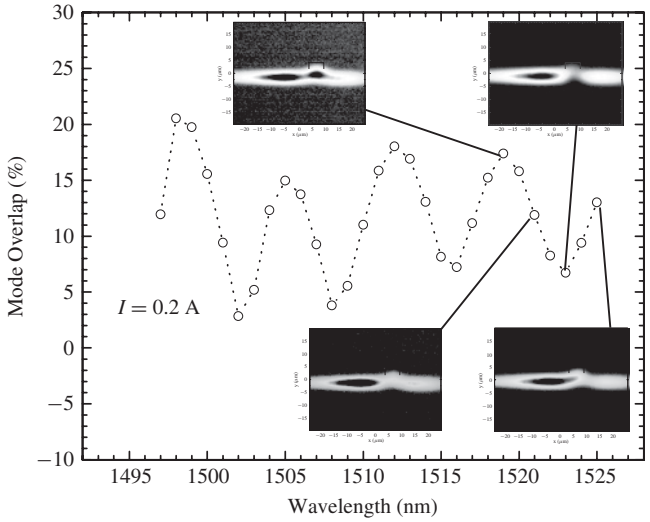

Fig. 7. Overlap calculation between the first higher order mode and a lensed-fiber mode illustrating effects of mode beating on coupling efficiency. Near-field images with ridge structure are also shown for wavelengths of 1519, 1521, 1523, and 1525 nm. The tested benchtop SCOWA was biased at 0.2 A and maintained at a temperature $T = 16$ ºC.

The near-field images show a strong beating phenomenon similar to the interaction of modes in a multimode interference coupler. The asymmetry between the left and right lobes of the higher order modes is most likely due to the effects of imaging an angled facet. In Fig. 7, the position of the waveguide ridge is indicated on the near-field modes. At 1519 nm, the intensity in the ridge is at a maximum as the fundamental and higher order modes add in phase. At 1523 nm, the phases of the modes are destructive, and the intensity cancels to nearly zero in the ridge. This interference causes the coupling to modulate in wavelength for these low bias currents. It should be noted that the near-field converges toward a single fundamental mode if the SCOWA is operated at either longer wavelengths or higher current biases as seen in Fig. 8. This is expected since higher order modes are cut off at longer wavelengths. Also, at higher current biases, the coupled mode filtering is stronger due to a larger gain difference between fundamental and higher order modes. The $1/e^2$ diameters of the mode are 5.5 and 7.8 μm.

TABLE II
CALCULATED SCOWA COUPLING EFFICIENCIES INTO THE FUNDAMENTAL MODE

Wavelength (nm)	1460	1470	1480	1490	1500	1510	1520	1530	1540	1550	1560	1570	1580
η_{in} (%)	73.5	72.0	75.0	75.5	81.5	84.5	86.0	90.0	90.0	90.0	90.0	90.0	90.0

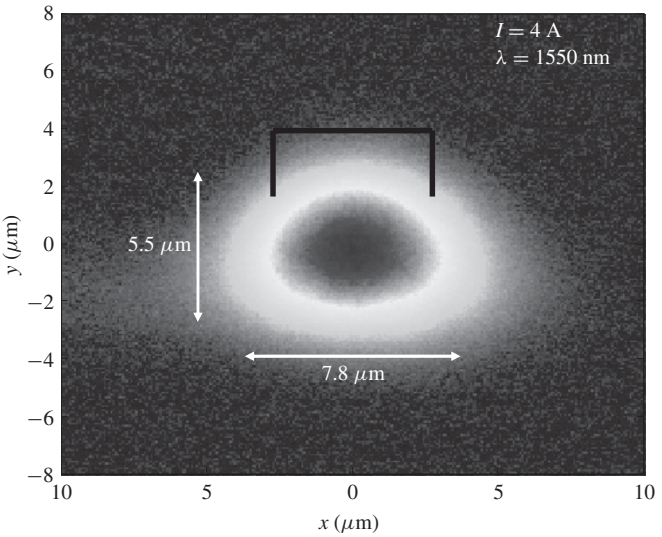

Fig. 8. Near-field image with ridge structure of the benchtop SCOWA operated at 1550 nm wavelength and 4 A current bias. The SCOWA was maintained at $T = 16$ °C.

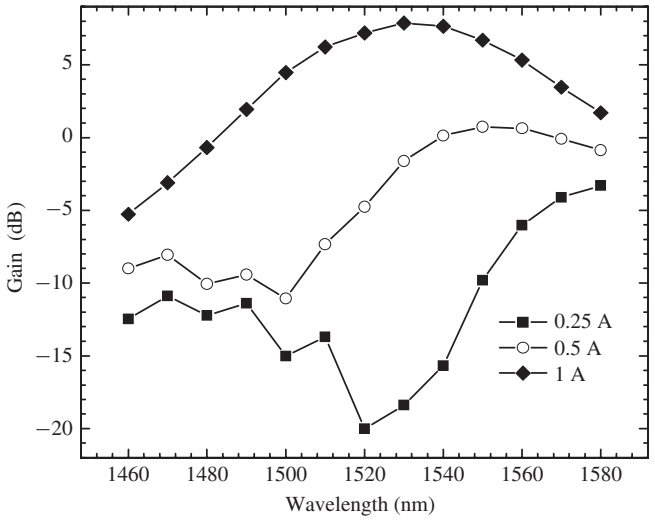

Fig. 9. Packaged SCOWA low bi as gain spectra for current biases of 0.25 A (solid squares), 0.5 A (open circles), and 1 A (solid diamonds). The temperature was maintained at $T = 16$ ℃.

These higher order mode coupling effects can also be observed in the low-bias gain spectra of the packaged SCOWA shown in Fig. 9. Usually, the gain is expected to decrease at shorter wavelengths since the inversion is weaker. However, the SCOWA gain is seen to increase for λ less than 1520 and 1500 nm for biases of 0.25 and 0.5 A, respectively. We believe that this abnormal gain behavior occurs because: 1) the higher order modes experience less overlap with the lossy active region compared to the fundamental mode, and 2) coupling to and from the higher order modes increases at shorter wavelengths. The spiking behavior in the gain spectra agrees strongly with that of Fig. 7 and is again attributed to the effects of mode interference on output coupling.

The n_{sp} values estimated from the NF data at 1, 3, and 5 A biases accounting for effects of input coupling loss due to higher order modes are also shown in Fig. 6. The increased input coupling loss η_{in} primarily affects the shorter wavelengths as expected, based on our previous discussion. In these calculations, an output coupling efficiency of 90% was still used since higher order modes are expected to be filtered out at these current levels. The value of η_{in} at each wavelength was determined by minimizing the difference between the 2-A n_{sp} curves estimated using the NF and *I–V* measurements. These same input coupling efficiencies (see Table II) were then used for η_{in} in the other bias conditions. The coupling efficiency at 1520 nm was independently calculated by finding the overlap between a measured 1520-nm mode of the benchtop SCOWA at 0 A bias with a lensed-fiber mode. At 0 A bias and 1520 nm wavelength, the intensity of the higher order modes is expected to dominate over the intensity of the fundamental mode. The calculated mode overlap was 3.8%, which matches well with the estimated 4% (90–86%) higher order mode coupling efficiency found from Table II.

The open squares in Fig. 6 show the n_{sp} estimated using NF measurements accounting for both effects of IVBA and coupling. The dashed lines in the figures show the n_{sp} calculated using *I–V* accounting for carrier heating. The agreement between the two curves is good for all bias currents tested. It should be mentioned that the variation in η_{in} needed for an exact match between the NF and *I–V* n_{sp} data was also examined. At each wavelength, the variation in η_{in} across all the current biases was $<5\%$.

V. DISCUSSION

In the previous sections, we justified that IVBA, carrier heating, and input coupling loss all contribute to degradation in NF by verifying the effects of each mechanism on n_{sp}. However, the NF is ultimately the parameter of interest as it determines the noise performance of the optical amplifier. We now relate degradation in n_{sp} to degradation in NF and show how IVBA, carrier heating, and input coupling loss affect NF. Fig. 10 illustrates the effect of each of the parameters on the NF of the packaged SCOWA at 5 A bias. An increase in IVBA loss is seen to cause a nearly uniform increase in NF. This occurs because the gain bandwidth of the SCOWA is >100 nm such that loss affects all tested wavelengths of the gain nearly equally. The gain spectrum, however, is not completely flat, and the gain still decreases slightly at longer

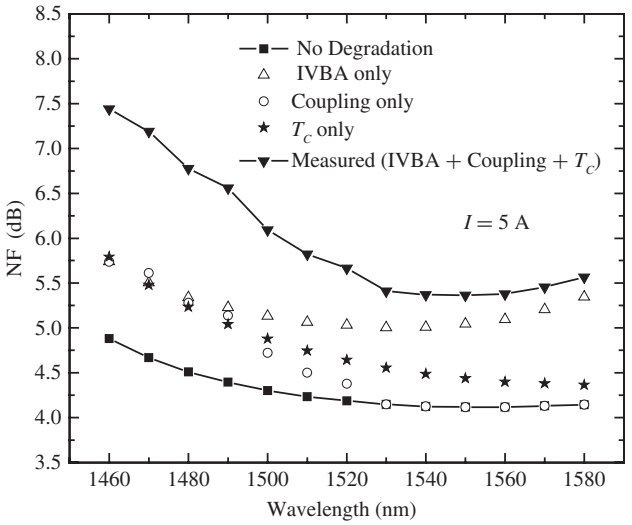

Fig. 10. Illustration of the impact of IVBA loss (open triangles), carrier heating (solid stars), and coupling loss (open circles) effects on NF. The SCOWA was operated under 5 A bias smallsignal conditions and cooled at $T = 16$ ºC.

wavelengths. As a result, a marginally larger increase in NF can be observed at those wavelengths. In contrast, coupling efficiency degradation primarily affects the short wavelength side of the spectrum where coupling into the fundamental mode is least efficient. The effect of coupling to quasi-bound modes turns on for $\lambda < 1520$ nm and is negligible at longer wavelengths. Finally, Fig. 10 shows that the effect of carrier heating similarly increases NF primarily at shorter wavelengths where population inversion is weakest. However, a small increase in NF due to carrier heating is also observed at longer wavelengths. The contributions from IVBA, input coupling loss, and carrier heating result in a ~2-dB increase in SCOWA NF. The remaining NF above 3 dB results from intrinsic amplifier properties of $\alpha_i = 0.5$ cm^{-1}, $\eta_{in} = 90\%$, and $T_c = 298$ K. Over the tested wavelength range, the total measured NF remains below 7.5 dB when the packaged SCOWA is operated at 5 A bias. The SCOWA thus exhibits phenomenal output power and NF performance along with reasonable gain over a bandwidth >100 nm.

VI. Conclusion

The NF of a packaged SCOWA was measured and verified using both optical and electrical domain approaches. The SCOWA exhibited 5.5 dB NF, 12.8 dB gain, and 0.8 saturation output power at 1550 nm operated at 5 A with a >100 nm gain bandwidth. The population inversion factor was extracted from the NF measurement and from measured *I–V* data. These measurements show that IVBA loss effects and carrier heating may present severe limitations to the noise performance of InGaAsP SOAs. IVBA effects can be reduced by increasing the barrier height to achieve higher confinement of electrons and holes. Carrier heating can be minimized by reducing the lattice temperature with appropriate high thermal conductivity submounts. Another potential option is to increase QW strain in order to reduce Auger recombination effects. The appearance of quasi-bound higher order modes can degrade coupling efficiency at shorter wavelengths, narrowing the bandwidth of device operation. This coupling loss can be decreased through optimization of the SCOW waveguide structure. Despite these limitations, the SCOWA demonstrates excellent signal amplification characteristics for high-power low-noise applications.

Appendix A
Derivation of (11)

The NF of an optical amplifier can be written as

$$NF = \chi\left(\frac{K\gamma\, P_{ASE,measured}}{Gh\nu B_o} + \frac{1}{G}\right) \tag{A1}$$

where h is the Planck constant, ν is the optical frequency, and B_o is the optical bandwidth. K accounts for the SOA polarization dependence, γ accounts for the output path loss, and χ accounts for wavelength dispersion effects. We first write $P_{ASE,measured}$ in (A1) in terms of measured total noise and laser noise as

$$P_{ASE,measured} = P_{noise\_total} - GP_{SSE} \tag{A2}$$

where P_{noise_total} is the total noise including both ASE and source spontaneous emission (SSE), G is the SOA gain accounting for coupling, and P_{SSE} is the SSE power. Substituting $P_{ASE,measured}$ in (A2) into (A1), we find

$$NF = \chi\left(\frac{K\gamma\,\left(P_{noise\_total} - GP_{SSE}\right)}{Gh\nu B_o} + \frac{1}{G}\right). \tag{A3}$$

If dispersion is present, the polarization of the signal and SSE arriving at the input of the amplifier will be detuned relative to the amplifier's optimal polarization. In this case, the NF can be expressed as

$$NF' = \chi\left(\frac{K\gamma\,\left(P'_{noise\_total} - G'P'_{SSE}\right)}{G'h\nu B_o} + \frac{1}{G'}\right) \tag{A4}$$

where the prime symbol denotes each respective quantity when the polarization is misaligned. Since both signal and noise are amplified by the gain, G' can be expressed in terms of SSE as

$$G' = \frac{G_{TE}P'_{SSE,TE} + G_{TM}P'_{SSE,TM}}{P'_{SSE}}. \tag{A5}$$

$G_{TE(TM)}$ is the amplifier TE TM gain, and $P'_{SSE,TE(TM)}$ is the laser SSE in the TE TM state. $G_{TM} < 0$ in an SCOWA at normal operating currents, and any polarization rotation of signal and noise into the TM state is effectively lost. P'_{noise_total} can be similarly expressed in terms of the ASE and measured values of G and SSE as

$$P'_{noise\_total} = P_{ASE} + G_{TE}P'_{SSE,TE} + G_{TM}P'_{SSE,TM}. \tag{A6}$$

Inserting (A5) and (A6) into (A4), we find

$$NF' = \chi\left(\frac{K\gamma\, P_{ASE}}{G'h\nu B_o} + \frac{1}{G'}\right). \tag{A7}$$

The numerator is unaffected by polarization rotation as one might expect for ASE. In comparing (A7) with the standard equation for NF

$$NF = \frac{K\gamma P_{ASE}}{Gh\nu B_o} + \frac{1}{G} \tag{A8}$$

we find

$$\chi = \frac{G'}{G} = \frac{G_{detuned}}{G_{aligned}}. \tag{A9}$$

REFERENCES

[1] K. Morito and S. Tanaka, "Record high saturation power (+22 dBm) and low noise figure (5.7 dB) polarization-insensitive SOA module," *IEEE Photon. Technol. Lett.*, vol. 17, no. 6, pp. 1298–1300, Jun. 2005.

[2] W. Xing, Y. Su, L. Xiang, J. Leuthold, and S. Chandrasekhar, "10-Gb/s RZ-DPSK transmitter using a saturated SOA as a power booster and limiting amplifier," *IEEE Photon. Technol. Lett.*, vol. 16, no. 6, pp. 1582–1584, Jun. 2004.

[3] T. Akiyama, M. Ekawa, M. Sugawara, H. Sudo, K. Kawaguchi, A. Kuramata, H. Ebe, K. Morito, H. Imai, and Y. Arakawa, "An ultrawide-band (120 nm) semiconductor optical amplifier having an extremely-high penalty-free output power of 23 dBm realized with quantum-dot active layers," in *Proc. Opt. Fiber Commun. Conf.*, vol. 2. Los Angeles, CA, Feb. 2004, pp. 1–3.

[4] P. W. Juodawlkis, J. J. Plant, L. J. Missaggia, K. E. Jensen, and F. J. O'Donnell, "Advances in 1.5-μm InGaAsP/InP slab-coupled optical waveguide amplifiers (SCOWAs)," in *Proc. IEEE Lasers Electro-Opt. Soc.*, Lake Buena Vista, FL, Oct. 2007, pp. 309–310.

[5] P. W. Juodawlkis, J. J. Plant, W. Loh, L. J. Missaggia, K. E. Jensen, and F. J. O'Donnell, "Packaged 1.5-μm quantum-well SOA with 0.8-W output power and 5.5-dB noise figure," *IEEE Photon. Technol. Lett.*, vol. 21, no. 17, pp. 1208–1210, Sep. 2009.

[6] P. W. Juodawlkis, J. J. Plant, R. K. Huang, L. J. Missaggia, and J. P. Donnelly, "High-power 1.5-μm InGaAsP-InP slab-coupled optical waveguide amplifier," *IEEE Photon. Technol. Lett.*, vol. 17, no. 2, pp. 279–281, Feb. 2005.

[7] J. P. Donnelly, R. K. Huang, J. N. Walpole, L. J. Missaggia, C. T. Harris, J. J. Plant, R. J. Bailey, D. E. Mull, W. D. Goodhue, and G. W. Turner, "AlGaAs-InGaAs slab-coupled optical waveguide lasers," *IEEE J. Quantum Electron.*, vol. 39, no. 2, pp. 289–298, Feb. 2003.

[8] D. M. Baney, P. Gallion, and R. S. Tucker, "Theory and measurement techniques for the noise figure of optical amplifiers," *Opt. Fiber Technol.*, vol. 6, no. 2, pp. 122–154, Apr. 2000.

[9] L. A. Coldren and S. W. Corzine, *Diode Lasers and Photonic Integrated Circuits*. New York: Wiley, 1995.

[10] T. Briant, P. Grangier, R. Tualle-Brouri, A. Bellemain, R. Brenot, and B. Thedrez, "Accurate determination of the noise figure of polarization-dependent optical amplifiers: Theory and experiment," *J. Lightw. Technol.*, vol. 24, no. 3, pp. 1499–1503, Mar. 2006.

[11] *CIP Technologies, SOA Application Note*. (2008) [Online]. Available: http://www.ciphotonics.com/

[12] A. Crottini, F. Salleras, P. Moreno, M. A. Dupertuis, B. Deveaud, and R. Brenot, "Noise figure improvement in semiconductor optical amplifiers by holding beam at transparency scheme," *IEEE Photon. Technol. Lett.*, vol. 17, no. 5, pp. 977–979, May 2005.

[13] G. E. Obarski and J. D. Splett, "Transfer standard for the spectral density of relative intensity noise of optical fiber sources near 1550 nm," *J. Opt. Soc. Am. B*, vol. 18, no. 6, pp. 750–761, 2001.

[14] M. Movassaghi, M. K. Jackson, V. M. Smith, and W. J. Hallam, "Noise figure of erbium-doped fiber amplifiers in saturated operation," *J. Lightw. Technol.*, vol. 16, no. 5, pp. 812–817, May 1998.

[15] Y. Sun, J. W. Sulhoff, A. K. Srivastava, J. L. Zyskind, C. Wolf, T. A. Strasser, J. R. Pedrazzani, J. B. Judkins, R. P. Espindola, A. M. Vengsardar, and J. Zhou, "An 80 nm ultra wide band EDFA with low noise figure and high output power," in *Proc. 23rd Eur. Conf. Opt. Commun.*, vol. 5. Edinburgh, U.K., Sep. 1997, pp. 69–72.

[16] G. Keiser, *Optical Communications Essentials*. New York: McGraw-Hill, 2003.

[17] F. Pommereau, R. Brenot, J. Landreau, L. L. Gouezigou, O. L. Gouezigou, O. L. Lelarge, F. Martin, F. Poingt, B. Rousseau, G.-H. Duan, and B. Thedrez, "Realisation of semiconductor optical amplifiers with homogeneous carrier density and low noise factor," in *Proc. Int. Conf. Indium Phosphide Relat. Mater.*, May 2005, pp. 102–105.

[18] C. Henry, "Theory of spontaneous emission noise in open resonators and its application to lasers and optical amplifiers," *J. Lightw. Technol.*, vol. 4, no. 3, pp. 288–297, Mar. 1986.

[19] C. Henry, R. Logan, F. Merritt, and J. Luongo, "The effect of intervalence band absorption on the thermal behavior of InGaAsP lasers," *IEEE J. Quantum Electron.*, vol. 19, no. 6, pp. 947–952, Jun. 1983.

[20] G. Fuchs, J. Horer, A. Hangleiter, V. Harle, F. Scholz, R. W. Glew, and L. Goldstein, "Intervalence band absorption in strained and unstrained InGaAs multiple quantum well structures," *Appl. Phys. Lett.*, vol. 60, no. 2, pp. 231–233, Jan. 1992.

[21] W. S. Ring, A. R. Adams, P. J. A. Thijs, and T. Van Dongen, "Elimination of intervalence band absorption in compressively strained InGaAs/InP 1.5 μm MQW lasers observed by hydrostatic pressure measurements," *Electron. Lett.*, vol. 28, no. 6, pp. 569–570, Mar. 1992.

[22] W. S. Ring, "Examination of intervalence band absorption and its reduction by strain in 1.55 μm compressively strained InGaAs/InP laser diodes," *Electron. Lett.*, vol. 30, no. 4, pp. 306–308, Feb. 1994.

[23] V. Mikhaelashvili, N. Tessler, R. Nagar, G. Eisenstein, A. G. Dentai, S. Chandrasakhar, and C. H. Joyner, "Temperature dependent loss and overflow effects in quantum well lasers," *IEEE Photon. Technol. Lett.*, vol. 6, no. 11, pp. 1293–1296, Nov. 1994.

[24] S. Seki, H. Oohashi, H. Sugiura, T. Hirono, and K. Yokoyama, "Study on the dominant mechanisms for the temperature sensitivity of threshold current in 1.3-μm InP-based strained-layer quantum-well lasers," *IEEE J. Quantum Electron.*, vol. 32, no. 8, pp. 1478–1486, Aug. 1996.

[25] J.-N. Fehr, M.-A. Dupertuis, T. P. Hessler, L. Kappei, D. Marti, F. Salleras, M. S. Nomura, B. Deveaud, J.-Y. Emery, and B. Dagens, "Hot phonons and Auger related carrier heating in semiconductor optical amplifiers," *IEEE J. Quantum Electron.*, vol. 38, no. 6, pp. 674–681, Jun. 2002.

[26] T. Chin-Yi, T. Chin-Yao, R. M. Spencer, L. Yu-Hwa, and L. F. Eastman, "Nonlinear gain coefficients in semiconductor lasers: Effects of carrier heating," *IEEE J. Quantum Electron.*, vol. 32, no. 2, pp. 201–212, Feb. 1996.

William Loh (S'10) received the B.S. degree in electrical engineering from the University of Michigan, Ann Arbor, in 2007, and the M.S. degree in electrical engineering from the Massachusetts Institute of Technology (MIT), Cambridge, in 2009. He is currently pursing the Ph.D. degree in electrical engineering at MIT.

His current research interests include high-power semiconductor amplifiers and lasers and studies of noise processes in semiconductor optical devices.

Jason J. Plant received the B.S. degree in physics and the M.S. degree in applied physics (optical sciences) from the University of Massachusetts Lowell, Lowell, in 1999 and 2001, respectively.

He is currently an Associate Staff Member in the Electro-Optical Materials and Devices Group, Lincoln Laboratory, Massachusetts Institute of Technology, Lexington, where he is involved in the fabrication, packaging, and characterization of advanced optoelectronic components. His current research interests include development of monolithic semiconductor mode-locked lasers, high-power semiconductor lasers and optical amplifiers, semiconductor external-cavity lasers, hybrid silicon-III/V integration, and quantum cascade lasers.

Jonathan Klamkin (S'06–M'09) received the B.S. degree in electrical and computer engineering from Cornell University, Ithaca, NY, in 2002, the M.S. degree in electrical and computer engineering, and the Ph.D. degree in electronic materials from the University of California, Santa Barbara, in 2004 and 2008, respectively.

He joined the Electro-Optical Materials and Devices Group, Lincoln Laboratory, Massachusetts Institute of Technology, Lexington, in 2008, where he is a member of the technical staff. His current research interests include directly modulated frequency-stabilized slab-coupled optical waveguide lasers, GaN-based optical modulators, microwave photonic subsystems, high power photodiode arrays, and photonic integration techniques including quantum well intermixing for novel photonic integrated circuits and devices.

Joseph P. Donnelly (S'60–M'63–SM'88–F'90–LF'05) received the B.S. degree from Manhattan College, Bronx, NY, and the M.S. and Ph.D. degrees from Carnegie Mellon University, Pittsburgh, PA, all in electrical engineering.

He is currently a Senior Staff Member at Lincoln Laboratory, Massachusetts Institute of Technology, Lexington. Before joining Lincoln Laboratory, he was the North Atlantic Treaty Organization Post-Doctoral Fellow at Imperial College London, London, U.K. In addition to his position at Lincoln, he was until recently an Adjunct Professor in the Physics Department, University of Massachusetts Lowell, Lowell. He was a National Lecturer for the IEEE Electron Devices Society in 1979. His current research interests include high-power semiconductor lasers, integrated optics, and avalanche photodiodes.

Dr. Donnelly is a member of the Bohmesche Physical Society, Eta Kappa Nu, and Sigma Xi. In 2001, he was a Guest Associate Editor for a special issue of the IEEE JOURNAL OF SELECTED TOPICS IN QUANTUM ELECTRONICS ON SEMICONDUCTOR LASERS, and from 2002 to 2004 an Associate Editor of the IEEE JOURNAL OF QUANTUM ELECTRONICS.

Frederick J. O'Donnell received the A.S. degree in electrical engineering from the Northeastern University, Boston, MA, in 1977.

He joined Lincoln Laboratory, Massachusetts Institute of Technology, Lexington, in 1973, where he is currently an Assistant Staff Member in the Electro-Optical Materials and Device Group. His current research interests include optical device testing, process development, and device fabrication for a variety of III–V materials.

Rajeev J. Ram (SM'07) received the B.S. degree in applied physics from the California Institute of Technology, Pasadena, in 1991, and the Ph.D. degree in electrical engineering from the University of California, Santa Barbara, in 1997.

He is currently a Professor at the Massachusetts Institute of Technology, Lexington, where he is Associate Director of the Research Laboratory of Electronics and Director of the Center for Integrated Photonics Systems. His current research interests include physical optics and electronics, including the development of novel components and systems for communications and sensing, novel semiconductor lasers for advanced fiber-optic communications, and studies of fundamental interactions between electronic materials and light.

Paul W. Juodawlkis (S'86–M'86–SM'06) received the B.S. degree from Michigan Technological University, Houghton, the M.S. degree from Purdue University, West Lafayette, IN, and the Ph.D. degree from the Georgia Institute of Technology, Atlanta, all in electrical engineering.

He was a Technical Staff Member at Lincoln Laboratory, Massachusetts Institute of Technology (MIT), Lexington, from 1988 to 1993, where he was a Hardware Systems Engineer on a multisensor airborne testbed program. He then joined the Ultrafast Optical Communications Laboratory, Georgia Institute of Technology. In 1999, he rejoined the Lincoln Laboratory, MIT, as a member of the Electro-Optic Materials and Devices Group. He is currently an Assistant Group Leader of the Electro-Optic Materials and Devices Group at the Lincoln Laboratory, where he is leading research on semiconductor optoelectronic devices and microwave photonics. His current research interests include development of optical sampling techniques for photonic analog-to-digital converters, quantum-well electrorefractive modulators, high-power waveguide photodiodes, high-power semiconductor optical amplifiers and their application in mode-locked lasers, and narrow-linewidth external-cavity lasers.

Dr. Juodawlkis is the Program Co-Chair of the 2010 Conference on Lasers and Electro-Optics. He has served as a Chair of the IEEE Photonics Society Technical Committee on Microwave Photonics from 2003 to 2006, Program Co-Chair of the 2003 Photonics Society Topical Meeting on Photonic Time/Frequency Measurement and Control, and committee member of the International Topical Meeting on Microwave Photonics in 2004 and 2008. He is a member of the Optical Society of America and the American Association for the Advancement of Science.